Analyst

Accepted Manuscript

ROYAL SOCIETY OF CHEMISTRY

www.rsc.org/analyst

An Instantaneous Colorimetric Protein Assay Based on Spontaneous Formation of Protein Corona on Gold Nanoparticles

Yan Teck Ho[1‡], *Barbara Poinard*[2,3†‡], *Eugenia Li Ling Yeo*[1], *James Chen Yong Kah*[1*]

[1]Department of Biomedical Engineering, National University of Singapore, Singapore

[2]Department of Biomedical Engineering, Arts et Métiers ParisTech, Paris, France

[3]Department of Biomedical Engineering, University of Paris Descartes, Paris, France

KEYWORDS

Gold nanoparticles, protein assay, protein corona, Bradford assay, Micro BCA assay

ABSTRACT

Commercial protein assays used ubiquitously in laboratories typically require long incubation times due to the inherently slow protein-reagent reactions. In this study, we report a novel facile technique for instantaneous measurement of total protein concentration by exploiting the rapid aggregation dynamics of gold nanoparticles (NPs). By adsorbing different amounts of protein on their surface to form a protein corona, these NPs can be sterically stabilized to different degrees from aggregation, thus exhibiting a spectrum of color change which can be quantitatively characterized by UV-Vis absorption spectroscopy. We evaluated this technique on four model proteins with different structures: Bovine Serum Albumin (BSA), Normal mouse Immunoglobulin G (IgG), Fibrinogen (FBG) and Apolipoprotein A-I (Apo-A1) using two approaches, sequential and simultaneous. We obtained an approach-dependent linear concentration range up to 80 μg/mL and 400 μg/mL for sequential and simultaneous approach respectively. This linear working range was wider than that of commercial Bradford assay and comparable to Micro BCA assay. The simultaneous approach was also able produce a linear working range of 200 to 1000 μg/mL ($R^2 = 0.995$) in human urine, while the sequential approach was non-functional in urine. Similar to Micro BCA, the NP-based protein assay was able to elicit a linear response ($R^2 > 0.87$) in all four proteins with different structures. However, unlike Micro BCA which require up to 120 min of incubation, we were able to obtain the read-out almost instantaneously without the need for incubation. The NP-based technique using the simultaneous approach can thus be exploited as a novel assay for instantaneous protein quantification to increase the productivity of laboratory processes.

INTRODUCTION

Protein assays are commonly used as bioanalytical tools to quantify total protein concentration in unknown biological samples. With advances in biotechnology that promise to increase the productivity of many laboratory experiments through high throughput assays that allow multiple read-outs simultaneously, there is a growing demand for assays to provide rapid read-outs while maintaining accuracy and sensitivity. However, many of the chemical or biological assays today are still limited by the chemical reaction rate inherent to the assay.

This is true for a wide range of protein assays such as Biuret, Bradford, micro-Bicinchoninic acid (Micro BCA), and Modified Lowry protein assays that are commercially available to perform quantitative proteomic analysis. These protein assays have in common a colorimetric scheme that produces a change in optical absorbance as a result of distinctive chemical reaction(s) between the proteins and the reagents in the specific assay. This final optical absorbance depends on the concentration of protein added. Proteins are thus quantified based on optical absorbance characteristics and compared against a calibrated standard. As with most protein-based chemistries, these chemical reactions are inherently slow and would often require an elevated temperature or relatively long incubation times ranging from 20 min at room temperature for Bradford assay to 120 min at 37 ºC for the Micro BCA protein assay kit.

Since the first reported use of gold nanoparticles (NPs) in colorimetric based detection[1], NPs have proven to be an effective alternative colorimetric agent for the detection of ions[2-5] and biological molecules[6-8]. There are two attributes of NPs that enabled these applications. First, NPs exhibit unique distance-dependent optical properties, where their surface plasmon resonance (SPR) changes according to their colloidal stability. This is translated to colorimetric changes as isolated NPs aggregate[9-11]. Second, the aggregation of NPs is easily induced by appropriate

surface ligands[12, 13] or ionic manipulation, such as when placed in high electrolyte concentration[14]. The aggregation can be rapid[15-17] due to their nanoscale dimension and associated high surface energy. Therefore, an appropriate aggregation-based strategy involving NPs would induce rapid colorimetric changes for detection of analytes.

NPs also present facile surface chemistry that allows attachment of many biomolecules or functional groups through both covalent and non-covalent interactions. In particular, NPs interact with proteins through a combination of electrostatic interactions, hydrophobic attraction and high affinity co-ordinate bonds with thiol or amine groups[18]. This results in the spontaneous formation of a protein corona when placed in biological media[19, 20]. While often considered a nuisance that obscures other useful surface functionalities, the protein corona has been shown to improve colloidal stability in some cases through steric stabilization[21]. They can also introduce biocompatible functionalities into NPs[22], be exploited for loading and triggered release of drugs[23, 24], and allow modulation of cellular responses[25].

Here, we exploit the spontaneous formation of protein corona as a tool for instantaneous quantification of protein concentration. We hypothesize that the extent of protein corona formed on NPs depends on the concentration of available proteins. By adsorbing different amount of proteins to form the protein corona, these NPs can be sterically stabilized from salt-induced aggregation to different degrees. When coupled to the colloidal stability-dependent optical property of NPs, a spectrum of quantifiable color changes from red for isolated NPs to purple or grey is produced, depending on the extent of aggregation. The reaction scheme of this NP-based protein assay is shown in Scheme 1.

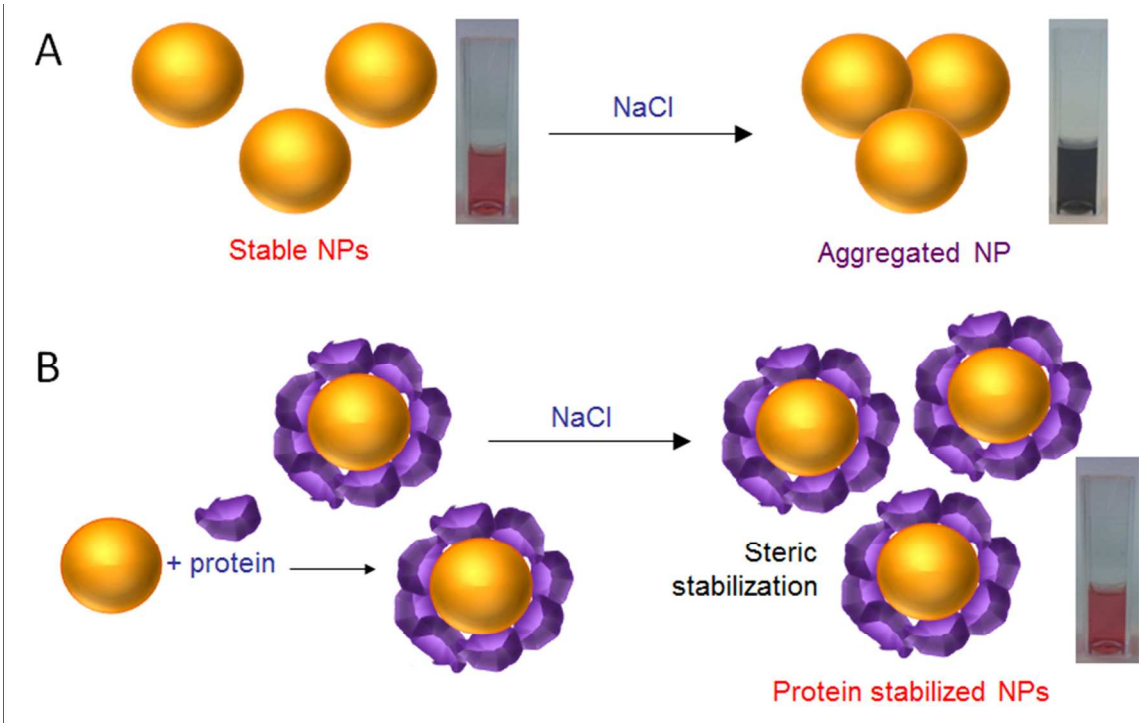

Scheme 1. Reaction schematic of the NP-based protein assay. (a) In the absence of protein, colloidally stable NPs aggregate in the presence of NaCl to result in a color change of colloidal NPs from red to purple. (b) In the presence of proteins, the adsorption of proteins on the NPs confers steric stabilization to the NPs and the colloidal NPs remain red in the presence of NaCl.

In this study, we report a facile and cost-effective technique for instantaneous measurement of protein concentration using two approaches: sequential and simultaneous approach. In the sequential approach, we first synthesized NPs and introduced them to four model proteins with different conformation: Bovine Serum Albumin (BSA), Normal Mouse Immunoglobulin (IgG), Fibrinogen (FBG) and Apolipoprotein A-I (Apo-A1). The NPs were then induced to aggregate by salt and the resulting color change was characterized by their UV-Vis absorption spectrum. The order of addition was changed in the simultaneous approach where the NPs were formed in the presence of proteins and salt. For both studies, the color change is calibrated against known

protein concentrations to determine the linear working range. We observed that the order in which the reactants were added was crucial towards the functionality and linear working range of the assay. We also compared the read-out of this NP-based assay with existing commercial protein assays.

The results of this study show that we can exploit the spontaneous formation of protein corona on NPs to enable rapid quantification of proteins that is comparable to existing commercial protein assays.

MATERIALS AND METHODS

Synthesis and characterization of NPs

All reactions were performed in 96-well microplates. We synthesized NPs rapidly by reducing hydrochloroauric acid ($HAuCl_4$, Sigma-Aldrich) with a strong reducing agent sodium borohydride ($NaBH_4$, Sigma-Aldrich). Briefly, 100 µl of 4 mM $NaBH_4$ was added to 100 µl of 1 mM $HAuCl_4$ at room temperature to form NPs in water instantaneously. The synthesized GNPs were characterized for their optical absorption using UV-Vis absorption spectroscopy (UV-2450, Shimadzu, Japan). The size, shape and morphology of NPs were examined using Transmission Electron Microscopy (TEM) (JEM-1220, JEOL Ltd., Japan). The hydrodynamic diameter, D_H from dynamic light scattering (DLS) and the zeta potential of the NPs were determined using the Zetasizer (Nano ZS, Malvern, UK). The synthesized NPs were prepared fresh for subsequent experiments.

Sequential approach to protein assay

In the sequential approach, the NPs were formed first, followed by the protein corona, before being induced to aggregate by salt. We synthesized the NPs as described earlier, before adding 50 µL of the proteins in buffer to 200 µL of the as-synthesized NPs. The mixture was shaken briefly for the protein corona to form spontaneously on the NPs[26, 27]. We chose purified Bovine Serum Albumin (BSA) (Thermo Fisher Scientific Inc.) in this study as our model protein to form the protein corona. Gel electrophoresis using a 0.5% agarose gel under 80V for 60 min was used to confirm the presence of corona layer on the NPs. Small aliquots of the BSA-coated NPs (NP-BSA) were also used to characterize the change in UV-Vis absorption spectrum (UV-2450, Shimadzu) and D_H (Nano ZS, Malvern) of the NPs after corona formation.

Following the brief incubation with proteins, the NPs were induced to aggregate by adding 50 µL of 100 mM sodium chloride (NaCl, Sigma-Aldrich) to the 250 µL of NP-BSA prepared earlier. This was followed by mild shaking for 5 seconds, which resulted in an instantaneous color change that correlated with the extent of aggregation. The aggregation was quantified from the UV-Vis absorption spectrum using the Multiskan GO Microplate Spectrophotometer (Thermo Scientific). All reactions were performed in triplicates for each protein concentration.

Simultaneous approach to protein assay

In the simultaneous approach, we mixed 50 µL of BSA with 50 µL of 100 mM NaCl and 100 µL of 100 mM $HAuCl_4$ at room temperature. The order of adding these reagents was not crucial to the functionality and performance of this approach. The solution was well mixed before 100 µL of 4 mM $NaBH_4$ was added to form the NPs almost instantaneously in the presence of proteins and NaCl. As the NPs were formed, the proteins stabilized them against salt-induced aggregation to varying degrees depending on the amount of proteins present. The color change

was characterized by UV-Vis absorption spectroscopy to quantify the extent of aggregation. All reactions were performed in triplicates for each protein concentration.

Protein concentration calibration curve

We used known standard concentrations of BSA (Pierce BSA standards, Thermo Fisher Scientific Inc.) commonly used in commercial protein assay kits to obtain the standard protein concentration calibration curve. The ratio of the NP's absorbance at 520 nm normalized to 580 nm (A520/A580) was used as a quantitative measure of their colloidal stability[28]. Isolated NPs typically possess a SPR absorbance peak at ~520 nm, with its intensity correlated to the concentration of NPs. As the NPs' absorbance at 580 nm is sensitive to aggregation[29], normalization to the absorbance at 580 nm allows us to quantify the NPs' colloidal stability in a concentration independent manner. A high A520/A580 value corresponds to a high degree of colloidal stability.

The A520/A580 was subsequently used to plot the concentration calibration curve of the NP-based protein assay. Using 50 µl of the protein solution, the A520/A580 of NPs was determined as a function of protein concentrations from 0 to 1000 µg/mL, from which we identified the linear working range. The linear concentration calibration curve was plotted for both sequential and simultaneous approaches. Apart from BSA, we also obtained the protein concentration calibration curve of IgG (Santa Cruz Biotechnology), FBG (Sigma-Aldrich) and Apo-A1 (Sigma-Aldrich) to examine the response characteristics of our NP-based assay to different proteins. The linear concentration calibration curves for all four proteins were compared between the two approaches of the NP-based assay and commercial protein assays.

The BSA concentration calibration curve was repeated in urine to examine the functionality of the NP-based assay in physiological media. The same BSA model protein of concentrations between 0 to 1000 μg/mL were reconstituted in an unadulterated urine sample obtained from a healthy volunteer, and used to obtain the concentration calibration curve for both sequential and simultaneous approaches as described previously. All reactions were performed in triplicates for each protein concentration.

Comparison with commercial protein assays

The linear concentration calibration curve of NP-based protein assay was compared to two commercial protein assays: Bradford (Quick Start Bradford protein assay, Bio-Rad) and Micro BCA (Thermo Scientific Micro BCA Protein Assay Kit, Pierce biotechnology) protein assay. Standard protocols in the kits were used in this study and standard concentrations of BSA were used as the calibration standards across all three protein assays. The experiments were performed in 96-well microplates in triplicates. After incubating the assays for the time specified in the kits, the absorbance was measured at 562 nm and 595 nm for Micro BCA and Bradford protein assays respectively. The concentration calibration curves were plotted and compared to the NP-based protein assay.

The reaction kinetics of NP-based protein assay was also compared to that of the Micro BCA and Bradford protein assay. The absorbance in each assay was read at fixed time points and the change in absorbance as a function of time was plotted for up to 120 minutes to determine the time taken for the assays to reach a constant absorbance that indicated the assays' end-point.

RESULTS AND DISCUSSION

Synthesis and characterization of NPs

Synthesis of NPs using $NaBH_4$ as a strong reducing agent resulted in instantaneous formation of NPs with size considerably smaller than the commonly synthesized citrate-capped NPs. Compared to conventional synthesis of citrate-capped NPs developed by Turkevich *et. al.* which requires at least 15 min of heating at 90 ºC to generate larger NPs (~20 nm)[30], the instantaneous synthesis of NPs is crucial for the NP-based protein assay to provide an instantaneous read-out. The NPs were monodisperse with a diameter of ~3 nm as determined from TEM, and a mean D_H of 4.42 nm, giving a SPR absorbance peak at 495 nm (Figure 1a and c). The zeta potential showed a surface charge of -22.4 mV, suggesting good colloidal stability even in the absence of stabilizing surface capping agents.

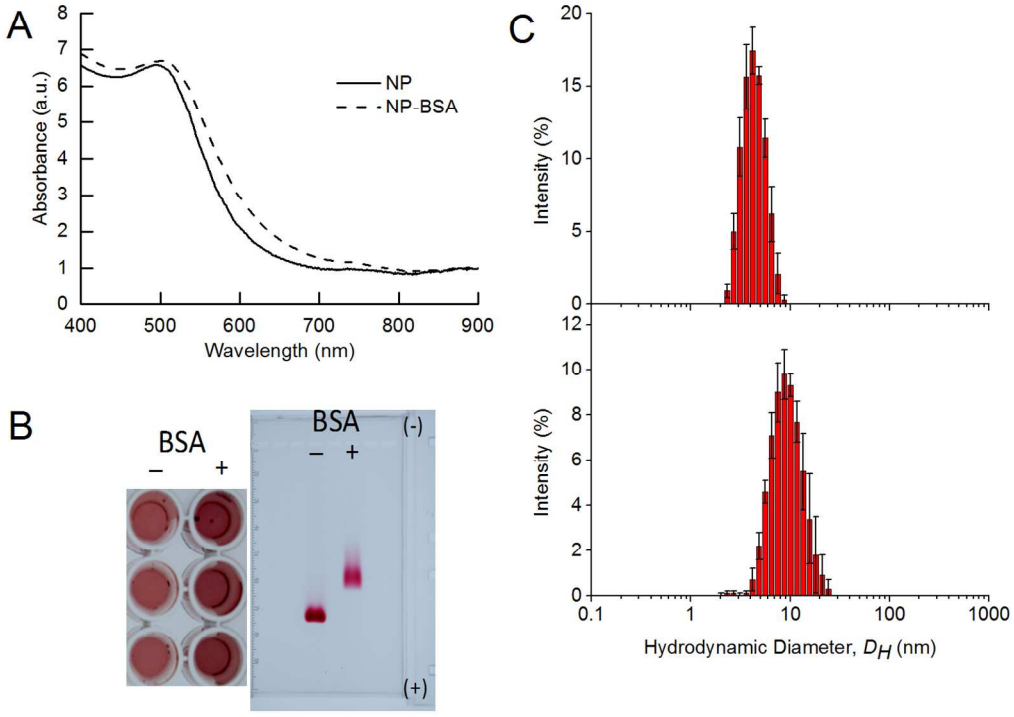

Figure 1. Sequential approach to spontaneous corona formation, showing the change in (a) UV-Vis absorption spectrum, (b) color of the NP colloid and band mobility in gel electrophoresis,

and (c) hydrodynamic diameter of NPs with the absorption and corona formation of BSA proteins. The three rows of wells in each image in (b) are triplicates of each other.

Sequential assay approach

In the sequential assay approach of the NP-based protein assay, we first synthesized the NPs, followed by forming the protein corona on the NPs, and then inducing aggregation using common salt. The addition of 50 µL of 50 µg/mL of BSA to the synthesized NPs caused a red-shift of 5 nm in the SPR peak from 495 nm to 500 nm (Figure 1a). This is typical of protein binding on the NP's surface, which causes a change in the dielectric environment of the NPs[31]. Although this did not lead to appreciable color changes in the solution (Figure 1b), we confirmed the binding of BSA around the NPs by a retardation of the mobility of NP's band towards the positive end under agarose gel electrophoresis.

The retardation of NP's band could be attributed to a change in either their D_H, zeta potential, or both. Here, both NPs and BSA-coated NPs (NP-BSA) migrated towards the positive end of the gel, indicating that both species are negatively charged. The formation of protein corona on the NPs also resulted in a change in zeta potential from -22.4 mV to -32.6 mV. Since the zeta potential measurements became more negative in the presence of BSA, we concluded that the increase in D_H from 4.42 nm to 9.75 nm (ΔD_H = 5.33 nm) due to binding of BSA to form the protein corona (Figure 1c) was responsible for the gel retardation. As BSA is a small globular protein of 67 kDa, the increase in D_H correlated well to the size of BSA molecules[32].

When 100 mM NaCl was added to the synthesized NPs in the absence of proteins, they aggregated irreversibly (Figure 2a, top row). This is in contrast to NP-BSA which remained as stable isolated NPs due to steric stabilization afforded by BSA (Figure 2a, bottom row)[33]. In

colloidal solutions, aggregation occurs when neighboring particles in close proximity overcome the energy barrier arising from electrical repulsion that exists as a result of like charges from the particles' zeta potential. Beyond this energy barrier, the particles fall into an energy trap that result in aggregation[34]. The aggregation of NPs caused the SPR peak absorbance in the UV-Vis spectrum to decrease significantly (Figure 2b, top row), resulting in a corresponding visual change in the colloidal solution from red to gray (Figure 2c, top row). The addition of NaCl to NP-BSA did not change the UV-Vis spectrum significantly, except for a slight red-shift in the SPR peak absorbance from 500 to 515 nm (Figure 2b, bottom row). This small change in the UV-Vis spectrum did not result in any significant color change in the colloidal solution (Figure 2c, bottom row). These results showed that the colorimetric difference could be used as a simple indicator for the presence of proteins.

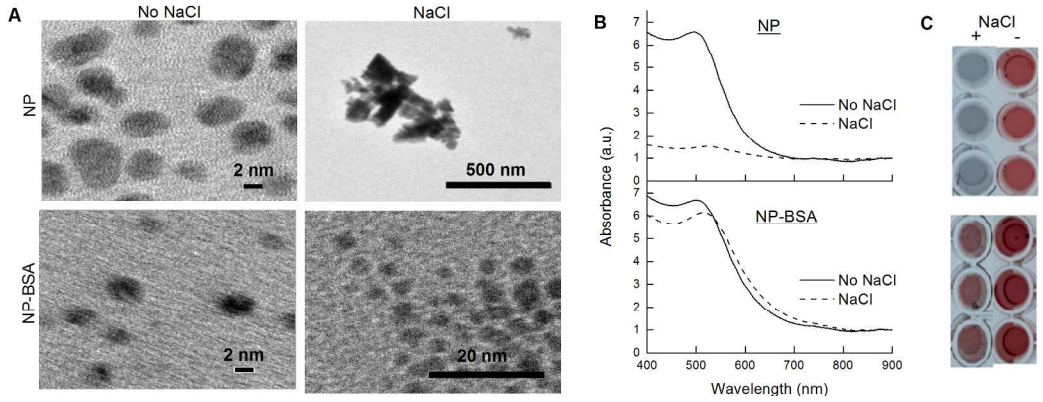

Figure 2. Colloidal stability of naked NPs and NPs with BSA protein corona (NP-BSA) formed from the sequential approach, after the addition of 100 mM NaCl. The aggregation of naked NPs by NaCl can be confirmed through the (a) TEM, (b) change in UV-Vis absorption spectrum, and (c) visual color change of the NP colloid (top row). In contrast, the NP-BSA remained stable in NaCl (bottom row). The three rows of wells in each image in (c) are triplicates of each other.

Simultaneous assay approach

The order of reagents added in the NP-based assay was changed in the simultaneous approach. Here, BSA and NaCl were added to $HAuCl_4$ and mixed prior to NPs synthesis. The $NaBH_4$ was then added to the mixture so that the NPs were formed in the presence of BSA and NaCl. We examined if this approach was also able to produce the same color change with NaCl-induced aggregation. In the absence of NaCl, very small NPs were formed in 50 µL of 200 µg/mL of BSA proteins. Such a protein-directed synthesis of NPs has also been reported and is known to produce BSA-conjugated NPs that possess both the fluorescence emission characteristics of gold nanoclusters and the SPR of gold nanoparticles[35].

The presence of BSA did not result in any observable shift in the SPR peak absorbance of NPs compared to that of NPs formed in the absence of BSA (Figure 3a). This did not lead to any observable color change in the NP colloidal solution, similar to the sequential assay approach (Figure 3b). However, the D_H increased from 3.43 nm to 6.30 nm (ΔD_H = 2.87 nm) as the NPs were formed in the presence of proteins under the simultaneous approach (Figure 3c). This increase was likely attributed to the adsorption of the BSA to form the protein corona, and was slightly smaller than that observed in the sequential approach (ΔD_H = 5.33 nm). This was probably due to smaller NPs being formed in the presence of proteins as evidenced from their SPR absorbance peak which was less pronounced than that from the sequential approach. Furthermore, protein-directed synthesis of NPs is also known to produce very small NPs [35].

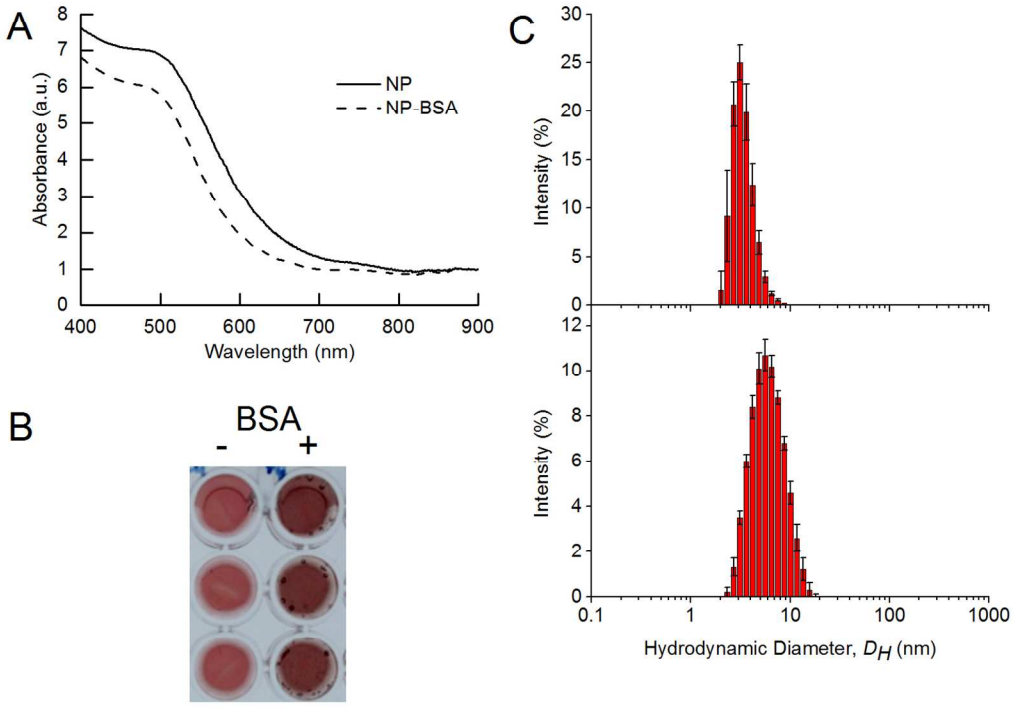

Figure 3. Simultaneous approach to spontaneous corona formation, showing the change in (a) UV-Vis absorption spectrum, (b) color of the NP colloid, and (c) hydrodynamic diameter of NPs with the absorption and corona formation of BSA proteins.

In the presence of 100 mM NaCl, the NPs formed without the BSA corona aggregated, while the NP-BSA remained stable as individual isolated nanoparticles, similar to the sequential approach (Figure 4a). In both approaches, the BSA corona was not visible under the TEM due to their weak electron absorption and response to the electron beam. In a similar manner as the sequential approach, the aggregation of NPs induced by NaCl caused the SPR peak absorbance in the UV-Vis spectrum of NPs to disappear (Figure 4b, top row), resulting in the colloidal NPs solution turning from red to grey (Figure 4c, top row). However, this decrease in the SPR peak absorbance was less pronounced for NP-BSA, and the peak absorbance merely red-shifted

slightly from 500 nm to 523 nm (Figure 4b, bottom row). Therefore, the change in the UV-Vis absorption spectrum did not lead to a significant visual change in the color of the colloidal solution (Figure 4c, bottom row). The simultaneous assay approach was also effective in detecting the presence of proteins around a colloidal solution of NPs.

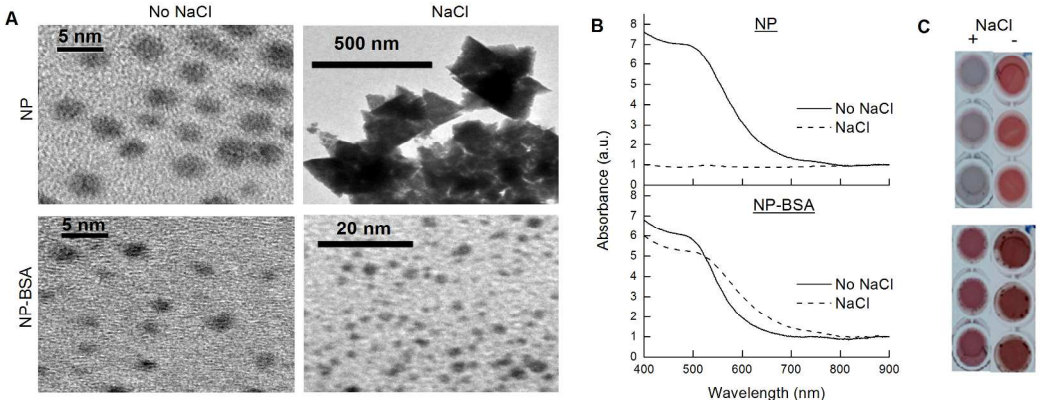

Figure 4. Colloidal stability of naked NPs and NPs with BSA protein corona (NP-BSA) formed from the simultaneous approach, after the addition of 100 mM NaCl. The aggregation of naked NPs by NaCl can be confirmed through the (a) TEM, (b) change in UV-Vis absorption spectrum, and (c) visual color change of the NP colloid (top row). In contrast, the NP-BSA remained stable in NaCl (bottom row). The three rows of wells in each image in (c) are triplicates of each other.

Protein concentration calibration curve

The protein concentration calibration curve forms the reference from which all unknown protein concentrations are determined. It is a plot of the optical absorbance in the protein assay against a range of known standard protein concentrations. The linear working range in this plot is the useful range where the protein concentrations can be determined accurately. Therefore, a wide linear range is often desirable in an assay to extend its utility over a wide range of protein concentrations. Instead of measuring the absorbance at a single wavelength, we used the

A520/A580 from the UV-Vis spectrum as a quantitative measure of the colorimetric change arising from NP's aggregation in our NP-based protein assay. The protein concentration calibration curve for the NP-based protein assay was determined with different standard concentrations of a working volume of 50 µL BSA.

Despite similar physical and optical properties, as well as colloidal stability of NP-BSA in NaCl, both sequential and simultaneous approaches of the NP-based protein assay produced different concentration calibration curves. In the sequential assay approach, as the concentration of BSA added to NPs was increased over a broad range from 0 to 1000 µg/mL, the NPs became increasingly more stable against NaCl-induced aggregation. The A520/A580 increased sharply with increasing BSA concentrations until about 100 µg/mL where the increase became marginal before little or no further increase was observed beyond 200 µg/mL (Figure 5a). This was probably due to the saturation of BSA on the NPs.

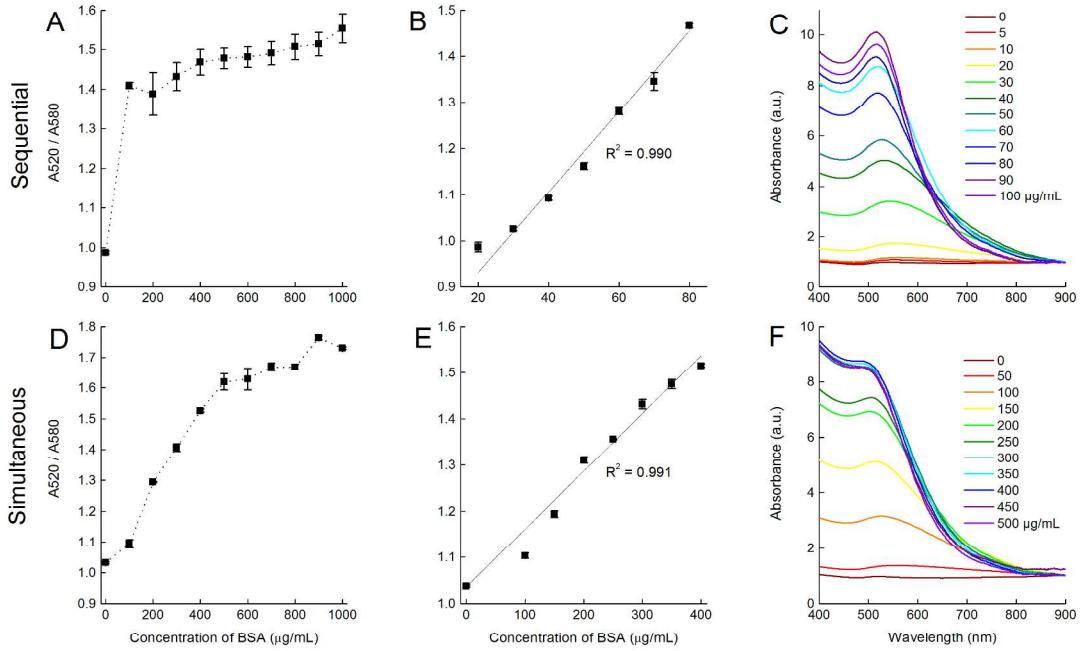

Figure 5. Protein concentration calibration curve of BSA obtained from the sequential (top) and simultaneous (bottom) approach. The curves were first determined from (a, d) a wide BSA concentration range from 0 to 1000 µg/mL, from which the (b, e) respective linear working range was then obtained together with the R^2 value. (c, f) The change in UV-Vis absorption spectrum with increasing BSA concentration for both approaches, from which the A520/A580 was derived.

We narrowed the range of protein concentrations to identify the linear working range. The sequential approach was able to achieve a linear response with $R^2 = 0.990$ from 20 to 80 µg/mL of BSA (Figure 5b). The UV-Vis absorption spectrum of NP-BSA after NaCl-induced aggregation showed a gradual increase in the SPR absorbance peak coupled with a slight blue-shift in the peak as the BSA concentration was increased (Figure 5c). These changes in the absorption spectrum resulted in the linear response range as the A520 increased much faster than A580. The NP-based assay showed a gradual color change from gray to purple to red, correlating to the increasing steric stabilization as the BSA concentration was increased.

In the simultaneous assay approach, the A520/A580 of NPs also increased with increasing BSA concentrations. However, unlike the sequential assay approach that is linear up to 80 µg/mL of BSA, the A520/A580 of NPs appeared linear from 0 to 400 µg/mL before saturation occurred (Figure 5d). This showed that the simultaneous assay approach could afford a wider linear working range of up to 400 µg/mL compared to the sequential assay approach. A plot of this linear working range from 0 to 400 µg/mL showed that the simultaneous assay approach was able to achieve a linear regression line with $R^2 = 0.991$ spanning a broad BSA concentration range from 0 to 400 µg/mL (Figure 5e).

The UV-Vis spectrum of the NPs also showed a gradual increase in the SPR absorbance peak coupled with a slight blue-shift in the peak as the concentration of BSA was increased (Figure 5f), although the SPR absorbance peak of NPs from the simultaneous assay approach was less pronounced than that of the sequential approach. This was due to smaller NPs produced from the simultaneous approach as discussed earlier. The difference in size was translated to a different color transition in the assay from gray to yellow to orange correlating to increasing extent of steric stabilization as the concentration of BSA was increased.

These results suggested that both sequential and simultaneous assay approach were able to provide a linear calibration of BSA concentrations based on their colorimetric response. However, by varying the sequence of addition of the various reactants in the assay, we were able to obtain different linear working ranges between the two approaches. As shown earlier, the simultaneous approach resulted in NPs with a smaller size compared to the sequential approach. Here, the BSA was added before the reducing agent so the proteins would bind to the NPs as soon as the NPs were formed. The BSA adsorption did not merely confer steric stabilization of NPs in the presence of NaCl, but also exerted an inhibitory effect on the growth of the NPs. This technique has been exploited by others to prepare ultra-small gold nanoclusters[35-37]. The smaller NPs formed in the presence of proteins possessed a larger surface area-to-volume ratio, which resulted in a greater overall surface area available for protein adsorption. This extended the upper limit of the linear working range and allowed the simultaneous approach to achieve a wider linear working range for BSA up to 400 μg/mL compared to the sequential approach (up to 80 μg/mL).

Concentration calibration curve in urine

We have also obtained the BSA concentration calibration curve in human urine to demonstrate the utility of our NP-based protein assay in quantifying proteins in physiological fluids. Here, BSA was reconstituted in urine at a range of concentration from 0 to 1000 µg/mL, and the concentration calibration curve was obtained from both the sequential and simultaneous approach. The simultaneous approach was able to achieve a linear working range from 200 to 1000 µg/mL with R^2 value of 0.995 (Figure 6a). This range was wider than that obtained from BSA in buffer. The increase in A520/A580 with BSA concentration was reflected as a gradual color change in the assay from purple to red as BSA concentration was increased (Figure 6b, top). However, the sequential approach did not yield a linear fit between 0 and 1000 µg/mL (Figure 6a). The A520/A580 remained relatively constant and the assay remained purple with no change in color as the BSA concentration was increased (Figure 6b, bottom). These results suggested that the simultaneous approach of the NP-based protein assay was more robust to complex physiological media while the sequential approach was no longer functional.

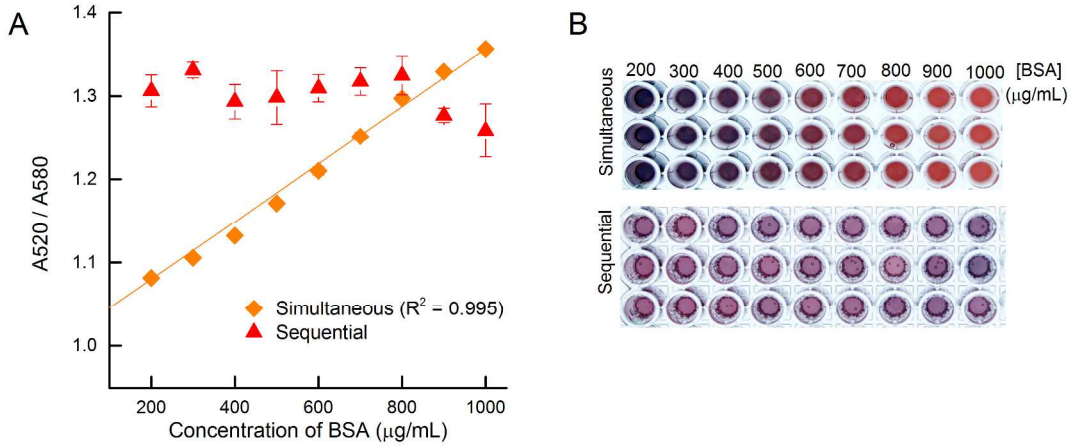

Figure 6. (a) Protein concentration calibration curves of BSA reconstituted in urine for both the simultaneous and sequential approach. The simultaneous approach had a linear working range of 200 to 1000 µg/mL (R^2 value of 0.995). The sequential approach did not show a linear

fit, with the A520/A580 constant over the range of BSA concentrations. (b) Photo of the simultaneous (top) and sequential (bottom) approach of the NP-based protein assay showing their color change at different concentrations of BSA in urine, with each row being the triplicates of each other. BSA concentrations was increased from left to right for each microplate.

Human urine contains many potentially interfering biochemical substances such as urea, uric acid and creatinine, and a high ionic content that can lead to indiscriminate aggregation of NPs[38]. It is therefore, not surprising that the NPs aggregated in urine even at high protein concentrations when the sequential approach was used. Here, the urine caused rapid aggregation of the NPs even before the proteins could form a stable corona around the NPs. However, when the NPs were formed in the presence of BSA and other nitrogen rich components in urine such as urea[39] in the simultaneous approach, these species simultaneously formed a stabilizing corona rapidly on the NPs as they were synthesized to prevent the NPs from aggregation.

The robustness of the NP-based protein assay in urine using the simultaneous approach demonstrated an advantage of this assay over commercial Micro BCA protein assay, where the presence of urea, along with other interfering components, are known to interfere with the bicinchonic acid reaction in Micro BCA unless the urine is pre-filtered to remove these interfering low molecular weight compounds[40].

It is possible that there may be other chemical species that could interfere with the NP-based protein assay. In reality, interference is a common problem faced by many commercial protein assays and many protein assays list their known interfering species for users to note. There are different approaches to minimize the effect of interfering species including removal by dialysis or gel filtration, sample dilution, and precipitating the proteins with cold acetone or

trichloroacetic acid (TCA). Therefore, these approaches could also be taken to minimize the effect of potential interfering species in the NP-based protein assay.

Comparison with linear working range of commercial assays

The protein concentration linear working range and color change of the NP-based protein assay were compared to two commonly used commercial protein assays: Bradford and Micro BCA protein assays, both of which also quantify protein concentrations based on colorimetric change. Standard protocols that came along with the kits were used to quantify protein in the micro assay format in 96-well plates with volumes less than 300 µL. The optical densities for Bradford and Micro BCA assays were measured at 595 nm and 580 nm respectively for protein quantification.

We first compared the protein concentration calibration curve of BSA for concentrations between 0 to 400 µg/mL. This was the linear working range of the NP-based protein assay determined earlier based on the simultaneous approach. Within this concentration range, only the Micro BCA protein assay showed a linear response ($R^2 = 0.979$) apart from the simultaneous approach of the NP-based assay ($R^2 = 0.991$) (Figure 7a). Both the Bradford protein assay and sequential approach of the NP-based assay suffered non-linearity beyond 50 µg/mL of BSA. In general, the Bradford assay is known to be linear over a short range, from 8 to 80 µg/mL for the microplate assay format[41, 42], often making dilutions of a sample necessary before analysis. Sample dilutions may introduce inaccuracies to measurements. While the sequential approach showed a compromised linear working range, the simultaneous approach of the NP-based assay showed a linear working range wider than that of commercial Bradford assay and comparable to

Micro BCA assay. Such a wide linear range is desirable for extending the utility of the assay over a wide range of protein concentrations without the need for repeated dilutions.

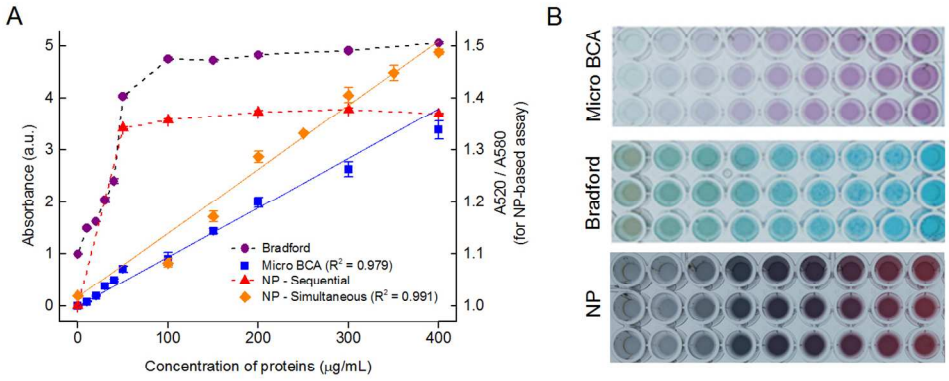

Figure 7. (a) Comparison of BSA concentration calibration curves between Bradford, Micro BCA, and NP-based protein assay for a concentration range of 0 – 400 μg/mL. Both the Micro BCA and NP-based assay using the simultaneous approach were able to exhibit a linear response within this range with R^2 = 0.979 and 0.991 respectively. The linear working range for Bradford and NP-based assay using the sequential approach was more limited and showed saturation at BSA concentration > 50 μg/mL. (b) Photo of the various protein assays showing their color change at different concentrations after their respective incubation time with each row being the triplicates of each other. BSA concentrations increase from left to right for each micro plate.

The BSA concentration calibration curves for both Bradford and Micro BCA protein assay (Figure 7a) was represented by a gradual absorbance change in a single dye color in the microplate. Here, the increase in BSA concentrations was coded by an increase in the blue and violet intensity for Bradford and Micro BCA protein assay respectively (Figure 7b, top two rows). Hence, their absorption was measured at only a single wavelength corresponding to the

peak absorption of the dye. In contrast, the NP-based protein assay (simultaneous approach) exhibited a gradual color change from gray to blue, purple, and red as the BSA concentration was increased (Figure 7b, bottom row). This was characterized by a peak shift in the UV-Vis absorption spectrum (Figure 5f). The measurement of absorption at a single wavelength was therefore insufficient to fully characterize the color change, so the ratio of absorption at 520 nm to 580 nm (A520/A580) was used as a quantitative measure of color change that correlated to protein concentration.

Response characteristics for different proteins

Commercial protein assays are known to have different calibration curves for different proteins. Here, we compare the protein concentration calibration curves for three other proteins with different structures: mouse IgG, FBG and Apo-A1 to examine the response characteristics of our NP-based assay to different proteins. The calibration curves were obtained from both sequential and simultaneous approach over a concentration range of 10 to 60 μg/mL, which had been shown earlier to give a linear response with BSA for both approaches (Figure 5b and 5e).

In the sequential approach, we were able to obtain a linear concentration calibration curve for all three proteins (R^2_{IgG} = 0.902, R^2_{FBG} = 0.981, $R^2_{Apo\text{-}A1}$ = 0.981), although the linear response for each protein was slightly different (Figure 8a). We attributed the variations in the calibration curve to differences in the size and structure of the proteins. While FBG is a large fibrous-like protein of 340 kDa consisting of a linear array of 3 nodules held together by a very thin thread[43], IgG is a smaller 150 kDa protein complex composed of two identical heavy chains and two identical light chains arranged in a Y-shape typical of antibody monomers. Apo-A1 is the smallest protein with molecular weight of 28 kDa that forms a hollow structure[44]. These

differences in molecular weight and conformation of different proteins would therefore affect the amount required by them to form a complete corona around the NPs. Nonetheless, the results indicated that the NP-based assay is applicable to different types of proteins if the purified sample of the target protein was used as the calibrating standard for the assay.

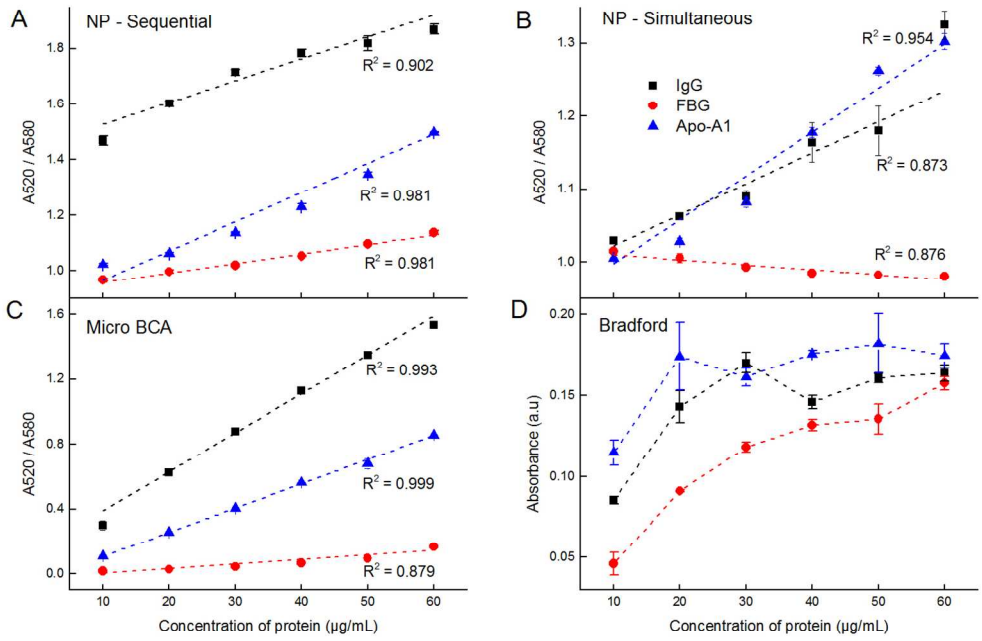

Figure 8. Protein concentration calibration curve of IgG, FBG and Apo-A1 obtained from the (a) Sequential, and (b) Simultaneous approach of the NP-based assay. This was compared to that obtained from commercial (c) Micro BCA and (d) Bradford protein assay. The linear fits (dashed lines) with R^2 values were shown for calibration curves with $R^2 > 0.87$.

Similar outcomes were also observed in the simultaneous assay approach, where all three proteins showed a linear response in their calibration curves with $R^2 > 0.87$ ($R^2_{IgG} = 0.873$, $R^2_{FBG} = 0.876$, $R^2_{Apo\text{-}A1} = 0.954$) (Figure 8b). However, instead of a linear increase with FBG

concentration, we observed an unexpected linear decrease in A520/A580 with increasing FBG concentration (Figure 8d, red circle). This was not observed for mouse IgG and Apo-A1. FBG is a protein involved in red blood cell (RBCs) aggregation and the coagulation cascade[9, 45], with higher levels of FBG associated with increased RBC aggregation due to its long fibrous-like structure[46]. This propensity of FBG to induce aggregation as it formed a corona during synthesis of NPs could have resulted in reduced colloidal stability of NPs at higher concentrations of FBG even in the absence of NaCl. This in turn led to the observed linear decrease in A520/A580 in the simultaneous approach.

In general, commercial protein assays also exhibit some degree of varying response toward different proteins. The documentation for Bradford assay stated a linear range of 1.2 to 10 µg/mL for BSA and 1.2 to 25 µg/mL for IgG in the microplate assay procedure (Bio-Rad Protein Assay, Bio-Rad Laboratories, Inc). We obtained the protein concentration calibration curves of the three models proteins (mouse IgG, FBG, and Apo-A1) for Micro BCA and Bradford protein assays as a comparison. Similar to the NP-based assay, Micro BCA was able to provide a linear response for all three proteins with $R^2 > 0.87$ ($R^2_{IgG} = 0.993$, $R^2_{FBG} = 0.879$, $R^2_{Apo\text{-}A1} = 0.999$), although the linear response for each protein was also different (Figure 8c). However, we were unable to obtain a linear response from Bradford assay for any of the proteins within the concentration range studied (Figure 8d). All three proteins showed saturation in the calibration curve beyond 30 µg/mL, thus further confirming the limited linear working range of Bradford protein assay as shown earlier.

The differences in the calibration curves amongst the three protein assays in this study can be explained from its functional mechanism. Most commercial protein assays typically quantify proteins based on biochemical reactions with functional groups in the proteins. Therefore,

differences between proteins are mainly due to biochemical factors, including differences in amino acid sequence, pI, composition in the primary structure of different proteins, number of peptide bonds in the proteins, pH of the reacting mixture in the assay, the protein tertiary and quaternary structures, or the presence of certain side chains or prosthetic groups. All these can dramatically alter the protein's color response. Here, Micro BCA is dependent on the number of peptide bonds present in the reaction mixture; Cu^{2+} ions found in Cupric sulphate pentahydrate in the working reagent of the assay is reduced to Cu^{+} by peptide bonds in the proteins, which is then chelated by bicinchoninic acid to form a purple solution that has strong absorbance at 562 nm. The final absorbance therefore, is dependent on the concentration of proteins present, which in turn affects the amount of Cu^{2+} ions being reduced. The working mechanism of Micro BCA is therefore less dependent on protein size and structure, but more dependent on its biochemistry.

On the other hand, the NP-based protein assay relied more on a physical mechanism of protein-induced steric stabilization on the NP surface. Differences in the calibration curve were more likely due to differences in protein size and structure, which affect their adsorption on NPs. The same is true for Bradford assay which is dependent on the protein's tertiary structure and consequently, its conformation[47].

In practice, most protein assays use BSA as the protein standard against which the concentration of protein in the sample is determined. However, the possibility of nuances in calibration curves with different proteins meant that the calibration curves obtained from BSA might not be directly applicable to other protein of interest whose concentrations we would like to measure. Therefore, better accuracy in quantifying an unknown concentration of a specific protein can be achieved if the purified sample of the target protein was used as the calibrating standard for the assay as discussed earlier.

Comparison of assay read-out time

We also compared the incubation time require for all three protein assays to achieve a stable and accurate quantitative read-out at three BSA concentrations. Most commercial protein assays require a long incubation time for the reaction to be completed based on standard protocols as specified in the kit. The time required for a protein assay to achieve a stable reading is also dependant on the protein concentration, with a higher concentration requiring shorter incubation time. At the lowest BSA concentration of 20 μg/mL, the absorbance from Micro BCA continued to increase even after 120 min of incubation time as specified by the protocol in the commercial kit (Figure 9, top, blue squares). There was no reduction in the incubation time needed to reach a stable absorbance even as the concentration of BSA was increased to 100 μg/mL (Figure 9, middle, blue squares). However, as the BSA concentration increased to 400 μg/mL, the required incubation time shortened to ~75 min to achieve a stable absorbance value (Figure 9, bottom, blue squares). While Micro BCA had a wide linear range of up to 400 μg/mL and was robust to different types of proteins, it was limited by a long incubation time required for an accurate quantification of protein concentration.

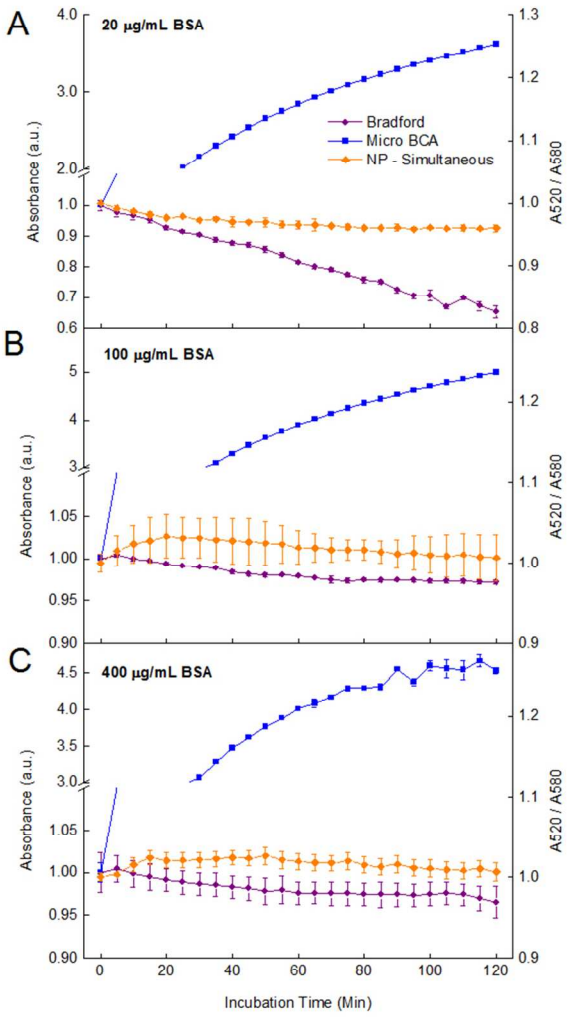

Figure 9. Comparison of reaction kinetics of Bradford, Micro BCA and simultaneous approach of the NP-based assay at (a) 20 µg/mL, (b) 100 µg/mL and (c) 400 µg/mL of BSA. The initial absorbance or A520/A580 of the assays at t = 0 min was normalized to 1, and the normalized absorbance or A520/A580 was plotted as a function of incubation time. Reaction stops when the absorbance or A520/A580 of the protein assays remains unchanged with time.

Compared to Micro BCA, Bradford protein assay was able to provide a rapid read-out with almost no incubation time needed to achieve a stable absorbance value at BSA concentration > 100 μg/mL (Figure 9, middle and bottom, purple circle). Such a rapid response was expected given that the protocol in the commercial kit specified at least 5 min of incubation. However, an unexpected decrease in the absorbance with time was observed for 20 μg/mL of BSA throughout the 120 min of incubation (Figure 9, top, purple circle). While Bradford assay exhibited rapid kinetics in read-out, this was only true for high concentrations of protein beyond its limited linear working range.

In contrast, the simultaneous approach of NP-based protein assay required almost no incubation time as the normalized A520/A580 achieved a relatively stable value almost instantaneously for all three BSA concentrations (Figure 9, orange diamonds). This suggested that the NP-based protein assay was instantaneous, which allowed the optical absorption to be measured almost immediately after the addition of the protein samples and the $NaBH_4$ reducing agent without requiring any incubation time. The NP-based assay was thus the only protein assay in our study that was instantaneous and yet exhibited a wide linear working range of up to 400 μg/mL, and was able to obtain a linear concentration calibration curve for all the proteins in this study.

CONCLUSION

In this study, we developed an instantaneous colorimetric assay for proteins based on spontaneous formation of protein corona on NPs. This NP-based assay can be implemented using either a sequential or simultaneous approach that differs in the order of addition of reactants. The simultaneous approach achieved a wider linear working range of up to 400 μg/mL compared to

the sequential approach with a linear range up to 80 μg/mL. The linear working range for simultaneous approach was wider than that of commercial Bradford assay and comparable to Micro BCA assay. The NP-based protein assay was also able to elicit a linear response (R^2 > 0.87) in all four proteins with different structures.

In comparison to commercial Bradford and Micro BCA protein assays, the NP-based assay offered both a wide linear working range and an instantaneous read-out that was not achieved by either Bradford or Micro BCA protein assay. Furthermore, the simultaneous approach in the NP-based assay demonstrated stability when calibrated with BSA (from 200 to 1000 μg/mL) in urine. Therefore, the NP-based protein assay represents a novel alternative to current state-of-the-art colorimetric assay that is instantaneous and yet cost effective. With further optimization, such a NP-based protein assay can be easy implemented in laboratories using commonly available chemicals to perform rapid initial screening of protein concentrations and increase the productivity of laboratory processes.

ASSOCIATED CONTENT

Supporting Information not available.

AUTHOR INFORMATION

Corresponding Author

*biekahj@nus.edu.sg

Present Addresses

†Current address: Department of Biomedical Engineering, National University of Singapore, 9 Engineering Drive 1, Block EA, #03-12, Singapore 117575.

Author Contributions

The manuscript was written through contributions of all authors. All authors have given approval to the final version of the manuscript. ‡These authors contributed equally.

Funding Sources

The funding used to support the research of the manuscript was from the Ministry of Education (MOE) AcRF Tier 1.

Notes

ACKNOWLEDGMENT

Funding was from the MOE AcRF Tier 1. We thank the NUS Electron Microscopy Unit for use of the TEM.

ABBREVIATIONS

REFERENCES

1. R. Elghanian, J. J. Storhoff, R. C. Mucic, R. L. Letsinger and C. A. Mirkin, *Science*, 1997, **277**, 1078-1081.
2. S. Kim, J. W. Park, D. Kim, D. Kim, I. H. Lee and S. Jon, *Angew Chem Int Edit*, 2009, **48**, 4138-4141.
3. S. P. Wu, Y. P. Chen and Y. M. Sung, *Analyst*, 2011, **136**, 1887-1891.
4. T. T. Lou, L. Chen, C. R. Zhang, Q. Kang, H. Y. You, D. Z. Shen and L. X. Chen, *Anal Methods-Uk*, 2012, **4**, 488-491.
5. S. K. Tripathy, J. Y. Woo and C. S. Han, *Nanotechnology*, 2012, **23**.
6. H. X. Li and L. Rothberg, *P Natl Acad Sci USA*, 2004, **101**, 14036-14039.
7. F. Xia, X. L. Zuo, R. Q. Yang, Y. Xiao, D. Kang, A. Vallee-Belisle, X. Gong, J. D. Yuen, B. B. Y. Hsu, A. J. Heeger and K. W. Plaxco, *P Natl Acad Sci USA*, 2010, **107**, 10837-10841.
8. T. E. Lin, W. H. Chen, Y. C. Shiang, C. C. Huang and H. T. Chang, *Biosens Bioelectron*, 2011, **29**, 204-209.
9. S. J. Everse, G. Spraggon, L. Veerapandian, M. Riley and R. F. Doolittle, *Biochemistry*, 1998, **37**, 8637-8642.
10. C. Guarise, L. Pasquato and P. Scrimin, *Langmuir*, 2005, **21**, 5537-5541.
11. M. Quinten and U. Kreibig, *Surf Sci*, 1986, **172**, 557-577.
12. C. Durand-Gasselin, M. Capelot, N. Sanson and N. Lequeux, *Langmuir*, 2010, **26**, 12321-12329.
13. H. Andresen, S. Gupta and M. M. Stevens, *Nanoscale*, 2011, **3**, 383-386.
14. H. Yang, X. P. Heng, W. Y. Wang, J. W. Hu and W. Q. Xu, *Rsc Adv*, 2012, **2**, 2671-2674.
15. K. Sato, K. Hosokawa and M. Maeda, *J Am Chem Soc*, 2003, **125**, 8102-8103.
16. N. Kanayama, T. Takarada and M. Maeda, *Chem Commun*, 2011, **47**, 2077-2079.
17. Y. Y. Xu, L. Deng, H. Wang, X. Y. Ouyang, J. Zheng, J. S. Li and R. H. Yang, *Chem Commun*, 2011, **47**, 6039-6041.
18. J. L. Burt, C. Gutierrez-Wing, M. Miki-Yoshida and M. Jose-Yacaman, *Langmuir*, 2004, **20**, 11778-11783.
19. T. Cedervall, I. Lynch, S. Lindman, T. Berggard, E. Thulin, H. Nilsson, K. A. Dawson and S. Linse, *P Natl Acad Sci USA*, 2007, **104**, 2050-2055.
20. M. H. Cui, R. X. Liu, Z. Y. Deng, G. L. Ge, Y. Liu and L. M. Xie, *Nano Res*, 2014, **7**, 345-352.
21. J. C. Y. Kah, A. Zubieta, R. A. Saavedra and K. Hamad-Schifferli, *Langmuir*, 2012, **28**, 8834-8844.
22. N. Wangoo, K. K. Bhasin, S. K. Mehta and C. R. Suri, *J Colloid Interface Sci*, 2008, **323**, 247-254.
23. J. C. Y. Kah, J. Chen, A. Zubieta and K. Hamad-Schifferli, *Acs Nano*, 2012, **6**, 6730-6740.
24. A. Cifuentes-Rius, H. de Puig, J. C. Kah, S. Borros and K. Hamad-Schifferli, *Acs Nano*, 2013, **7**, 10066-10074.
25. J. C. Kah, C. Grabinski, E. Untener, C. Garrett, J. Chen, D. Zhu, S. M. Hussain and K. Hamad-Schifferli, *Acs Nano*, 2014, **8**, 4608-4620.

26. E. Casals, T. Pfaller, A. Duschl, G. J. Oostingh and V. Puntes, *Acs Nano*, 2010, **4**, 3623-3632.
27. S. Tenzer, D. Docter, J. Kuharev, A. Musyanovych, V. Fetz, R. Hecht, F. Schlenk, D. Fischer, K. Kiouptsi, C. Reinhardt, K. Landfester, H. Schild, M. Maskos, S. K. Knauer and R. H. Stauber, *Nature nanotechnology*, 2013, **8**, 772-781.
28. S. Xiulan, Z. Xiaolian, T. Jian, J. Zhou and F. S. Chu, *International Journal of Food Microbiology*, 2005, **99**, 185-194.
29. C. De Roe, P. J. Courtoy and P. Baudhuin, *The journal of histochemistry and cytochemistry : official journal of the Histochemistry Society*, 1987, **35**, 1191-1198.
30. J. Turkevich, P. C. Stevenson and J. Hillier, *Discussions of the Faraday Society*, 1951, **11**, 55-75.
31. M. Iosin, F. Toderas, P. L. Baldeck and S. Astilean, *J Mol Struct*, 2009, **924–926**, 196-200.
32. S. H. Lacerda, J. J. Park, C. Meuse, D. Pristinski, M. L. Becker, A. Karim and J. F. Douglas, *Acs Nano*, 2010, **4**, 365-379.
33. S. Dominguez-Medina, J. Blankenburg, J. Olson, C. F. Landes and S. Link, *ACS sustainable chemistry & engineering*, 2013, **1**, 833-842.
34. R. J. Hunter, *Zeta potential in colloid science : principles and applications*, Academic Press, London; New York, 1981.
35. J. Lin, Z. Zhou, Z. Li, C. Zhang, X. Wang, K. Wang, G. Gao, P. Huang and D. Cui, *Nanoscale Res Lett*, 2013, **8**, 170.
36. J. P. Xie, Y. G. Zheng and J. Y. Ying, *J Am Chem Soc*, 2009, **131**, 888-+.
37. T. H. Chen and W. L. Tseng, *Small*, 2012, **8**, 1912-1919.
38. A. I. Nossier, S. Eissa, M. F. Ismail, M. A. Hamdy and H. M. E.-S. Azzazy, *Biosensors and Bioelectronics*, 2014, **54**, 7-14.
39. J. Du, B. Zhu and X. Chen, *Small*, 2013, **9**, 4104-4111.
40. B. Kirschbaum, *Clinical Chemistry*, 1986, **32**.
41. O. Ernst and T. Zor, *Journal of visualized experiments : JoVE*, 2010.
42. T. Zor and Z. Selinger, *Anal Biochem*, 1996, **236**, 302-308.
43. C. E. Hall and H. S. Slayter, *The Journal of biophysical and biochemical cytology*, 1959, **5**, 11-16.
44. Z. Wu, V. Gogonea, X. Lee, R. P. May, V. Pipich, M. A. Wagner, A. Undurti, T. C. Tallant, C. Baleanu-Gogonea, F. Charlton, A. Ioffe, J. A. DiDonato, K. A. Rye and S. L. Hazen, *J Biol Chem*, 2011, **286**, 12495-12508.
45. B. Blomback, B. Hessel, D. Hogg and L. Therkildsen, *Nature*, 1978, **275**, 501-505.
46. B. Neu and H. J. Meiselman, *Biophys J*, 2002, **83**, 2482-2490.
47. M. M. Bradford, *Anal Biochem*, 1976, **72**, 248-254.

Insert Table of Contents Graphic and Synopsis Here